Molecular Catalysis 446 (2018) 88–97

Contents lists available at ScienceDirect

Molecular Catalysis

journal homepage: www.elsevier.com/locate/mcat

H_2 photo-production from methanol, ethanol and 2-propanol: Pt-(Nb)TiO_2 performance under UV and visible light

Olga Fontelles-Carceller, Mario J. Muñoz-Batista, José Carlos Conesa, Anna Kubacka*, Marcos Fernández-García*

Instituto de Catálisis y Petroleoquímica, CSIC, C/Marie Curie, 2, 28049 Madrid, Spain

ARTICLE INFO

Article history:
Received 13 November 2017
Received in revised form
15 December 2017
Accepted 16 December 2017

Keywords:
Anatase
Doping
Quantum efficiency and yield
Selectivity
Rate

ABSTRACT

In this work we analyzed the photo-production of hydrogen using titania-based systems able to profit from UV and visible light photons. For this purpose, we prepared Niobium-doped titania and a titania reference by a microemulsion method, subjected these oxide precursors to calcination and subsequently introduced Pt as co-catalyst by a chemical reduction method. These materials were characterized in terms of the structural and morphological properties of the oxide and metal phases. Using these materials, we measured the reaction rate and quantum efficiency of the hydrogen photo-production using methanol, ethanol, and 2-propanol as sacrificial agents. Significant activity enhancement was observed in the Niobium-doped material with respect to the titania reference material. The study focuses on interpreting the differences presented (between the two samples) among the three alcohols in the hydrogen yield and provides a physico-chemical study to understand the roots of the activity. Such study was mainly based on the analysis of the reaction mechanism using in-situ infrared spectroscopy together with the analysis of the energetics of the reaction taking into account the fate of the sacrificial alcohol during reaction.

1. Introduction

Hydrogen appears as an energy vector potentially important for a future where greener and more sustainable chemical processes are required. This is due to the fact that the molecule is ideal to store energy (ca. 3 times more than conventional natural gas per unit volume) and does not generate toxic or dangerous molecules during its chemical transformation to release energy [1]. Production of hydrogen trough photocatalysis using light and particularly sunlight and bio-derived molecules such as alcohols can provide a sustainable and attractive path with neutral carbon emissions, leading to a greener future [2–9].

Titania corresponds to the most utilized material in photocatalysis due to its inherent properties related to a modest cost, limited toxicity and outstanding chemical properties under illumination. However, its use is limited to the UV electromagnetic region due to its wide band gap, always above 3.0 eV. The use of sunlight requires, in a first approximation, the efficient handling of photons corresponding to the visible light region [1–8]. In the context of the photocatalytic production of hydrogen, the use of visible photons without compromising UV performance has been achieved by a number of methods. A successful one is the doping of the anatase material with specific cations such as B, Fe, Nb, Ce and others. Using Pt or noble metals as co-catalyst, the above mentioned doped titania samples displayed significant activity in the reforming of alcohols under UV and/or visible illumination [10–16].

Several bio-alcohols have been tested in the literature as sacrificial agents in the photo-production of hydrogen highlighting the importance of several experimental variables in order to maximize the production of hydrogen. Among them we can highlight the co-catalyst chemical nature and physico-chemical properties, charge carrier handling by the metal-support system, alcohol:water ratio, or the light wavelength and intensity [17–33]. Methanol is the simplest molecule from the structural and chemical points of view and probably the molecule receiving most attention due to the relatively high hydrogen production rates commonly observed [14,15,34–37]. Irrespective of the alcohol chemical nature, the studies show that hydrogen molecules are essentially produced stoichiometrically from the alcohol, although the hydrogen atoms are exchanged through scrambling with the corresponding atoms of water molecules of the media during the production process of

* Corresponding authors.
E-mail addresses: ak@icp.csic.es (A. Kubacka), m.fernandez@icp.csic.es, mfg@icp.csic.es (M. Fernández-García).

https://doi.org/10.1016/j.mcat.2017.12.023
2468-8231/

the hydrogen molecule [36,38]. A schematic representation of the reactions that summarizes the most important chemical steps is as follows:

$$Cat + h\nu \rightarrow Cat + h^{+} + e^{-} \quad (1)$$

$$h^{+} + H_2O_{ads} \rightarrow OH^{\circ} + H^{+} \quad (2)$$

$$RCH_2OH_{ads} + h^{+}\,(OH^{\circ}) \rightarrow \text{Products} + \text{H}^{+}\,(H_2O) \quad (3)$$

$$2H^{+} + 2e^{-} \rightarrow H_2 \quad (4)$$

In brief, light absorption triggers the creation of electron and holes (Eq. (1)). These charge carriers reach the surface and produce several chemical species (Eqs. (2)–(4)). In the case of the alcohol reforming, holes or hole-related species such as hydroxyls are responsible of the attack (or oxidation) of the alcohol (Eq. (3)) while electrons are consumed in the production of hydrogen (Eq. (4)) [2–4]. A point usually dismissed in the literature is connected with the carbon-containing molecules produced in step 3. Hydrogen production depends critically on this issue or more specifically on the hydrogen remaining on the carbon-containing products due to the already mentioned stoichiometric relationship essentially holding between hydrogen production and hydrogen content of the sacrificial molecules [36,38].

Analysis of catalytic performance concerning the study of several alcohols as sacrificial agents has been presented for noble-metal promoted titania materials [25,39–41]. Alcohols having at least one hydrogen atom bonded to the (carbon) alpha position render higher reaction rates. Progress in understanding the differences in hydrogen production rates as a function of the alcohol nature showed the importance of alcohol polarity and the exponential of the alcohol potential oxidation in controlling the rate of hydrogen production [40,41]. However the understating of the physico-chemical interpretation of photo-activity in terms of alcohol chemical nature has not considered the chemical variable concerning the critical role that the different chemical products generated as a function of the alcohol chemical nature must have in hydrogen production. This point is obviously related to the chemical properties of the active centers transforming the alcohol sacrificial molecules.

In this contribution we study the hydrogen photo-production using several alcohols as sacrificial molecules and taking into account the use of UV and visible light illumination in order to progress in creating systems able to profit from sunlight. For this task we carried out a study using methanol, ethanol and 2-propanol and measured the reaction rates as well as the true quantum efficiency. Although all these molecules have hydrogen in alpha positions (to the hydroxyl moiety), significant differences in hydrogen photo-production rate are expected. We utilized titania and, more importantly, Niobium-doped titania as supports of the Pt-based catalysts in order to achieve high activity under both UV and visible illumination [14,15]. This work provides an interpretation of catalytic output concerning activity and selectivity of the alcohol photo-reforming reaction through an in-situ infrared analysis of the alcohol activation together with a thermodynamic analysis of the energy of the process and its connection with the hydrogen production rate.

2. Experimental

2.1. Preparation and characterization of catalysts

Materials were prepared using a microemulsion method by addition of Titanium tetraisopropoxide to an inverse emulsion containing either an aqueous solution of hydrated Niobium nitrate (Sigma) or just water dispersed in *n*-heptane, using Triton X-100 (Aldrich) as surfactant and hexanol as cosurfactant. Total cation content of the aqueous solution is 0.5 M. Water/(Ti+Nb) and water/surfactant molar ratios were, respectively, 111 and 18 for all samples. The resulting mixture was stirred for 24 h, centrifuged, decanted, rinsed with methanol and dried at 300 K for 6 h. Following the microemulsion preparation method, the amorphous powders were calcined under air for 2 h at 723 K. The co-catalyst was introduced subsequently by a chemical deposition method using a H_2PtCl_6 (Aldrich) solution. First, the calcined powder was suspended by stirring in a deionized water solution for 30 min. After that, the proper quantity of H_2PtCl_6 was added to the solution (to get a 0.5 wt.% of Pt on metal basis) and kept under stirring 5 min more. The reduction was carried out using a $NaBH_4$ (Aldrich) aqueous solution (Pt/$NaBH_4$ molar ratio 1/5). The final solid was rinsed with deionized water, collected by centrifugation and dried at 353 K. Samples are named Ti (Pt-TiO_2 reference system) and Nb (Pt-Nb doped-TiO_2). Niobium (when present) and Platinum content of the solids were measured with total reflection x-ray fluorescence (Bruker – S2 PicoFox TXRF Spectrometer) rendering values equal to 0.5 wt% for Pt in both catalysts and 2.5 mol% (cationic basis as $Nb_{0.025}Ti_{0.0975}O_x$) for the Nb sample within an error below 2.1and 1.5% for, respectively, Niobium and Platinum components.

XRD profiles of the samples were obtained using a polycrystal XíPert Pro PANalytical diffractometer using Ni-filtered Cu Kα radiation with a 0.02° step. Crystallite sizes reported were calculated from XRD patterns using the Williamson-Hall method which takes into account the strain and particle size contributions to the XRD peak broadening [42].The BET surface areas and average pore sizes and pore volumes were measured by nitrogen physisorption (Micromeritics ASAP 2010). UV–vis diffuse-reflectance spectroscopy experiments were performed on a Shimadzu UV2100 apparatus using $BaSO_4$ or Teflon as a reference, and the results presented as the Kubelka-Munk transform [43]. Band gap analysis for an indirect/direct semiconductor was done following standard procedures; e.g. plotting $(h\nu a)^n$ (n = ½ or 2 for indirect or direct semiconductor; hv = excitation energy, a = absorption coefficient, assumed to be proportional to the Kubelka-Munk transform in the relevant wavelength range) vs. energy and obtaining the corresponding intersection of the linear fit with the baseline [44].

Diffuse Reflectance Infrared Fourier Transform Spectra (DRIFTS) were taken in a Bruker Vertex 80 FTIR spectrometer using a MCT detector and running under OPUS/IR software. The set-up consists of a praying mantis DRIFTS accessory (Harrick Scientific) and a reaction cell (HVC, Harrick Scientific). The reaction mixture was prepared by injecting in a nitrogen carrier (50 mL min^{-1}) a 3:7 alcohol:water mixture (0.08 mL min^{-1}) with a syringe pump before entering the DRIFTS cell. The DRIFTS spectra were collected in the range of 4000–600 cm^{-1} with a resolution of 2 cm^{-1}, by averaging 10 scans over a total of 1.2 s. In DRIFTS experiments in-situ light excitation was carried out using 365 nm (488, 550 nm) radiation. A Hg-Xe 500 W lamp with a dicroic filter 280–400 nm coupled with a 365 nm (25 nm half-width) filter (LOT-Oriel) were used to select the light excitation. Each sample, without any previous treatment (expect flowing nitrogen for 10 min), was subjected in a continuous mode (without modifying gas mixture) to a single, multi-step experiment which aims to test the: *i)* adsorption of the reactive mixture under dark conditions, *ii)* reaction mixture evolution under illumination conditions, and *iii)* subsequent stay at dark conditions. Spectra were taken after different exposure times to verify any evolution behavior.

2.2. Description of reactor and catalytic outputs

Photocatalytic measurements at liquid medium were carried out using a cylindrical-type, batch pyrex (cutting absorption edge at ca. 300 nm) reactor of 4 cm depth (z coordinate in the numerical

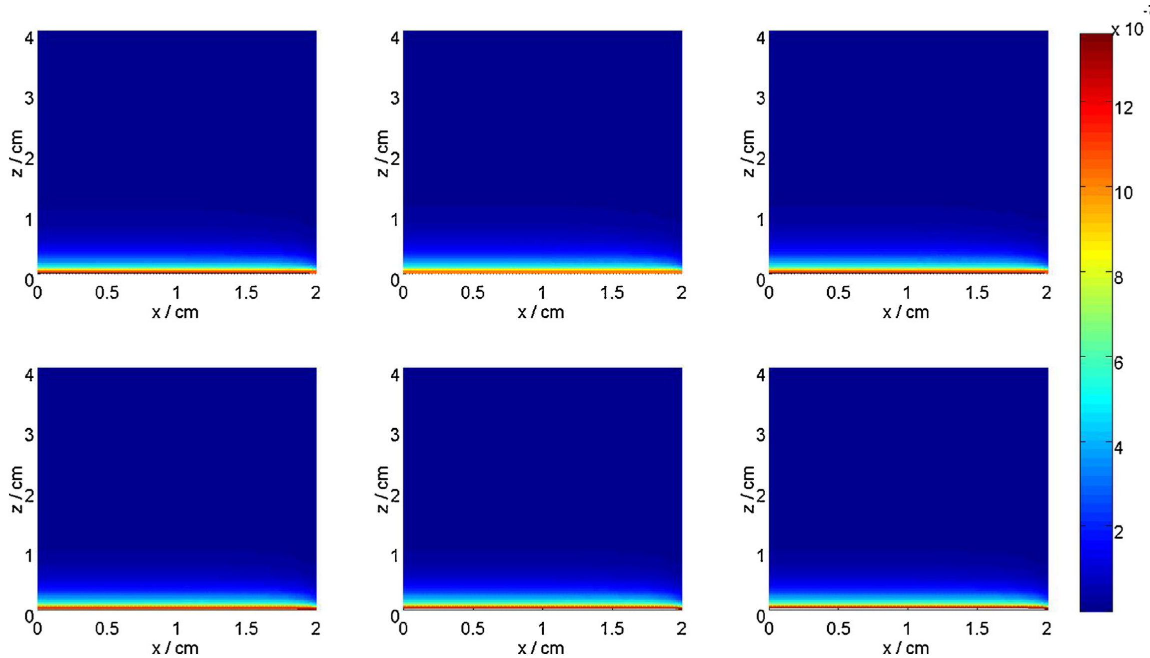

Fig. 1. Local volumetric rate of photon absorption (Einstein cm^{-3} s^{-1}) obtained under UV illumination for the Ti (upper panels) and Nb (lower panels) samples and concerning reaction with methanol (left column), ethanol (middle column) and 2-propanol (right column).

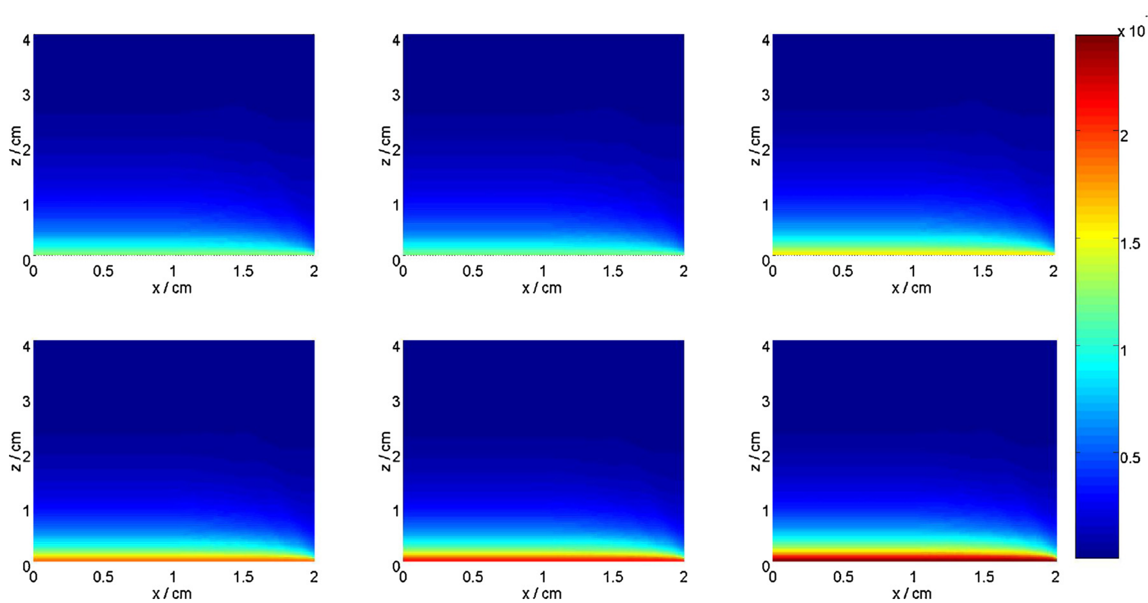

Fig. 2. Local volumetric rate of photon absorption (Einstein cm^{-3} s^{-1}) obtained under Visible illumination for the Ti (upper panels) and Nb (lower panels) samples and concerning reaction with methanol (left column), ethanol (middle column) and 2-propanol (right column).

analysis) and circular section with a 2 cm radius (r coordinate; for details see Ref. [14]). The reactor is filled with ca. 50 mL of a suspension of the catalyst in 3:7 (v/v) RCH_2COH/H_2O mixture medium maintained at a constant temperature (293 ± 1 K). The ratio is chosen to provide maximum activity according to previous reports [14]. The catalyst suspension (0.5 g L^{-1}) was first degassed with an Ar stream for around 20 min. Subsequently, the Ar flow was settled down to 10 mL min^{-1} and stabilized before reaction. Ar is used as carrier to displace reaction gases from the reactor to the detection system. The solution inside the reactor was irradiated from above using a Hg-Xe lamp (500 W) and dichroic filters (LOT Quantum Design) allowing exposure of the catalysis to the UV (280–400 nm) or Visible (420–680 nm) wavelength range. The reaction rates for hydrogen production were evaluated at 3 h from the start of the irradiation, where a pseudo-stationary situation is reached. The hydrogen production rate was analyzed using an on-line Mass spectrometry (Onmistart 300), gas (TCD/FID detection using HP-PLOT-Q/HP-Innowax columns and an Agilent 6890 apparatus) and liquid chromatography (xD8-C18/5 microm, 4.6×150 mm Agilent HPLC Column Eclipse and a Varian Pro Star 230 apparatus).

Quantum efficiency was calculated, according to the IUPAC recommendation [45], as the ratio of the number of molecules reacting by the number of photon interacting with the sample (Eq. (5)).

$$\eta_q\,(\%) = 100 \times \frac{r\left(\mathrm{molm^{-3}s^{-1}}\right)}{S < e^{a,\nu} > \left(\mathrm{Einsteinm^{-3}s^{-1}}\right)} \tag{5}$$

The reaction rate of hydrogen production (r in Eq. (5)) is divided by the selectivity factor (S) and the averaged local volumetric photon absorption rate ($<e^{a,\nu}>$). The so-called selectivity factor (dimensionless) is calculated as a summation over all chemical reactions generating protons (Eq. (3)) and takes the value:

$$S = \sum_{i} n_i S_i \quad (6)$$

Where S_i is the fractional selectivity to product i, and n_i is the inverse of number of charge carrier species required to obtain one mol of hydrogen [46].

To determine the denominator, we also need to obtain the solution of the radiative transfer equation (RTE; Eq. (7)) in the heterogeneous reactor(s). The RTE for liquid phase measured the variation of radiation intensity (associated to a beam of rays at wavelength λ in the direction of a solid angle vector, $\underline{\Omega}$) through a direction of the space (s) [47].

$$\frac{dI_{\lambda,\underline{\Omega}}\left(\underline{x}\right)}{ds} = -\kappa_\lambda I_{\lambda,\underline{\Omega}}\left(\underline{x}\right) - \sigma_\lambda I_{\lambda,\underline{\Omega}}\left(\underline{x}\right) + \frac{\sigma_\lambda}{4\pi} \int_{\Omega'=4\pi} p\left(\underline{\Omega}' \rightarrow \underline{\Omega}\right) I_{\lambda,\underline{\Omega}'}\left(\underline{x}\right) d\Omega' \quad (7)$$

Where κ_λ is the absorption coefficient; σ_λ is the scattering coefficient; and $p\left(\underline{\Omega}' \rightarrow \underline{\Omega}\right)$ is the scattering phase measured with the Henyey and Greenstein phase function, as usually done for titania samples [47]. κ_λ and σ_λ coefficients are obtained from transmittance and reflectance measurements in model suspensions of the catalysts [46,47]. Eq. (7) assumes that (i) the emission radiation is negligible (at room temperature), and (ii) steady state condition during the photocatalytic processes. Eq. (7) is solved using the discrete ordinate method and considering the corresponding boundary equations (known inlet radiation from the upper window and null reflection in the inner wall of the reactor surfaces, see Ref. [46] for details). Once the spatial and angular distribution of the intensity is obtained, the local volumetric rate of photon absorption ($e^{a,\nu}$) is calculated at each $r-z$ point of the reactor according to [14]:

$$e^{a,\nu}\left(\underline{x}\right) = \int_{\lambda} \kappa_\lambda \cdot \int_{\Omega=4\pi} I_{\lambda,\underline{\Omega}}\left(\underline{x}\right) d\Omega d\lambda \quad (8)$$

The $e^{a,\nu}\left(\underline{x}\right)$ parameter is presented for the Ti and Nb samples in Figs. 1 and 2 under, respectively, UV and visible illumination. In these figures a "r-z" section ($0 < r \leq 2$; $0 \leq z \leq 4$ cm) of the reactor is shown. The reactor volume is constructed from this section by the azimuthal symmetry around the central axis of the cylindrical reactor, having all sections equal values of the observable.

3. Results and discussion

The basic characterization of the two materials (Ti and Nb) is presented in Fig. 3 using XRD and UV–vis spectroscopy. The analysis of the corresponding XRD patterns and UV–vis spectra renders physico-chemical information summarized in Table 1. From the point of view of the titania support, Table 1 collects rather similar values for all observables for the two samples. The anatase structure (PDF 21-1272; space group $I4_1$/amd) of titania therefore displays equal morphological properties as well as band gap values. The physico-chemical analysis of the samples was completed using chemical analysis, XPS, microscopy and other techniques, described in a previous report [14]. For both samples, Pt has a similar primary crystallite size of ca. 1.3 ± 0.1 Å and, for the Nb sample, the Nb/Ti surface ratio measured by XPS took a value of 0.023:0.977 (rather close to the nominal one of 0.025:0.975).

The rate of hydrogen production using the two samples and illumination sources and the three alcohols tested here are presented in panel A of Fig. 4. As may be expected considering previous results

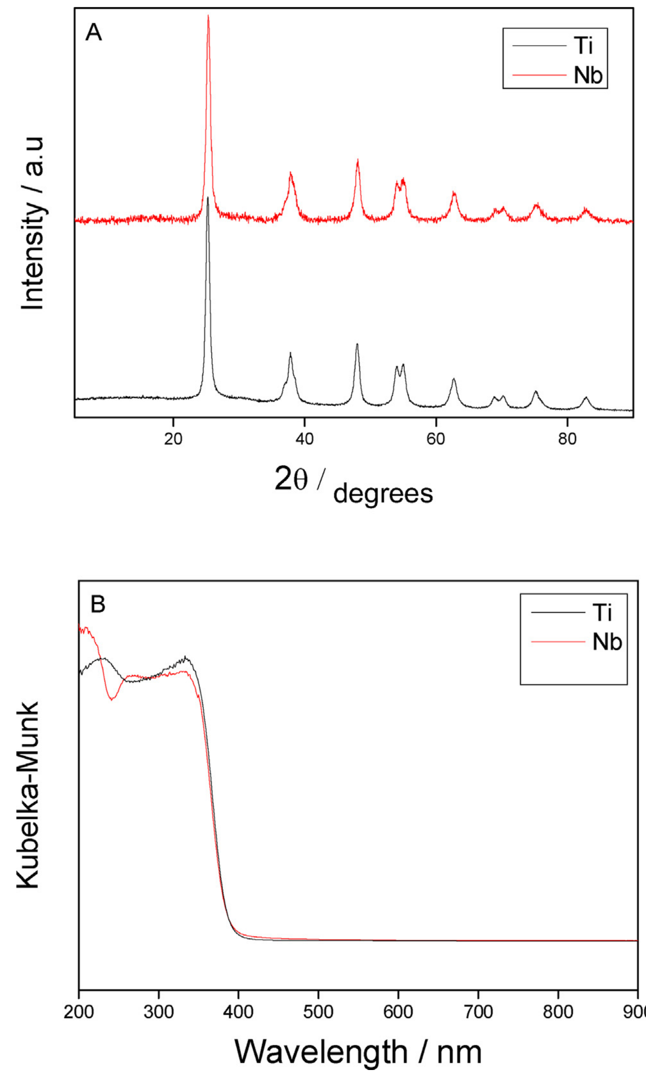

Fig. 3. XRD patterns (A) and UV–vis spectra (B) of the samples.

for titania-based materials [25,39–41], Ti and Nb samples present maximum rates for methanol, followed by ethanol and 2-propanol, irrespective of the illumination source. Larger differences using the three alcohols are observed for the Nb sample with respect to the Ti reference but the trend of both samples is rather similar. The selectivity of carbon containing products generated is summarized in Table 2. For methanol, both samples generate formic acid and metyl formate but the Nb sample also shows the production of formaldehyde under UV illumination. For ethanol in all illumination conditions both samples generate acetaldehyde and ethyl acetate. We did not detect carbon containing molecules originated from the fragmentation of the C_2^+ molecules detected. Finally, for 2-propanol larger differences are observed among our samples. The Nb sample generates acetone and propanone-diisopropyl-acetal while the Ti sample only renders acetone. Again no fragmentation is detected and only the mentioned C_3^+ products are detected. So, the presence of Niobium at the surface of the material makes small changes in the active centers as to trigger the generation of a few products not observed in the case of Ti. In any case and according to Table 2, these are minor products accounting only for no more than 20% of the alcohol molecules transformed. Note that CO_2 is not detected through all tests carried out (Table 2).

The balance equations required to generate the different carbon containing products are presented in Table 3. The different prod-

Table 1
Main physico-chemical properties of the catalysts.

Sample	Bandgap (eV)	Size (nm)	BET Area (m^2/g)	Pore volume (cm^3/g)	Pore size (nm)
Nb	3.15	11.9	80.5	0.131	5.6
Ti	3.18	12.3	82.1	0.129	5.5

Standard error: 0.04 eV; 0.5 nm; 3.0 $m^2 g^{-1}$.

Table 2
Carbon-containing products detected in the alcohols photo-transformation under UV and visible illumination.

Alcohol	Sample	Illumination	Product	Selectivity (%)[a]
Methanol	Nb	UV	Formic acid	85
			Formaldehyde	8
			Methyl formate	7
		Vis	Formic acid	91
			Methyl formate	9
	Ti	UV	Formic acid	90
			Methyl formate	10
		Vis	Formic acid	98
			Methyl formate	2
Ethanol	Nb	UV	Acetaldehyde	89
			Ethyl acetate	11
		Vis	Acetaldehyde	97
			Ethyl acetate	3
	Ti	UV	Acetaldehyde	81
			Ethyl acetate	19
		Vis	Acetaldehyde	71
			Ethyl acetate	29
2-propanol	Nb	UV	Acetone	74
			Propanone diisopropyl acetal	26
		Vis	Acetone	80
			Propanone diisopropyl acetal	20
	Ti	UV	Acetone	100
		Vis	Acetone	100

[a] Average Standard error; 4.6%.

Table 3
Standard Gibbs energy of formation of the alcohols and of the alcohol oxidation reactions.

Alcohol	$\Delta_f G^\circ$(J mol^{-1})	Balanced equation	(−)ΔG°(J mol^{-1})
Methanol	$-166.6 \cdot 10^3$	$CH_4O + 2h^+ \rightarrow CH_2O + 2H^+$	$64.1 \cdot 10^3$
		$CH_4O + 4h^+ + H_2O \rightarrow CH_2O_2 + 4H^+$	$42.3 \cdot 10^3$
		$2CH_4O + 4h^+ \rightarrow C_2H_4O_2 + 4H^+$	$-53.2 \cdot 10^3$
Ethanol	$-174.8 \cdot 10^3$	$C_2H_6O + 2h^+ \rightarrow C_2H_4O + 2H^+$	$47.2 \cdot 10^3$
		$2C_2H_6O + 4h^+ \rightarrow C_4H_8O_2 + 4H^+$	$16.9 \cdot 10^3$
2-propanol	$-180.3 \cdot 10^3$	$C_3H_8O + 2h^+ \rightarrow C_3H_6O + 2H^+$	$27.6 \cdot 10^3$
		$3C_3H_8O + 2h^+ \rightarrow C_9H_{20}O_2 + H_2O + 2H^+$	$155.4 \cdot 10^3$

ucts require a different number of (hole-related) charge carriers but as the number of charge carries consumed matches the number of protons generated, this simplifies significantly the calculation of the quantum efficiency as the S (selectivity) factor always takes a factor of 1/2. So, the reaction rate has to be multiplied by a factor of 2 as commonly carried out. This can be also seen easily considering Eq. (4). Using the S value and the average volumetric rate of photon absorption, we calculate the true quantum efficiency (Eq. (5)). Panel B of Fig. 4 summarizes the corresponding results. Under UV/visible illumination, maximum quantum efficiency values of 5.2/2.4 are obtained using methanol, 4.2/1.1 for ethanol, and 1.9/0.9 for 2-propanol. All these values correspond to the Nb sample, which displays quantum efficiency values between 1.8–2.8 times higher than those of the Ti reference sample. The trends observed for the reaction rate and quantum efficiency as a function of the sample (Nb vs. Ti) and illumination source are essentially the same, indicating that the reaction rate is in this case a good indicator of the "true" photo-activity of sample. Therefore, we can use the reaction rate in order to investigate the origin of activity differences among the alcohols tested.

To understand such issue, we first carried out an in-situ analysis of the alcohol photo-transformation using infrared spectroscopy. Only UV illumination results are presented due to the practical absence of significant changes with respect to visible illumination, although signals generated under reaction conditions were significantly weaker in the later case, likely due to the lower reaction rates. Note that considering the selectivity values collected in Table 2, an essentially identical mechanism is expected under all illumination conditions here tested. So, UV-DRIFT results are representative of all illumination conditions. In Figs. 5 and 6 an in-situ infrared study of the two catalysts was carried out by obtaining difference spectra taking as background the first spectrum recorded during each step (from *i* to *iii*) of the treatment of the samples consisting in a sequential: *i)* adsorption of the alcohol in presence of water vapour, *ii)* reaction mixture (alcohol:water) under illumination conditions, and *iii)* subsequent stay at dark conditions under the same reactive mixture used in previous steps of the experiment. Samples were not pre-treated prior IR measurements.

Adsorption of methanol prior to illumination provides evidence of the existence of methanol and methoxy species (upper row in Figs. 5 and 6). For Ti and Nb samples, methanol (C—H contributions at 2940/2831 and 2945/2836 cm^{-1}, respectively) seems to have larger intensity than methoxy (2920/2816 and 2920/2817 cm^{-1}, respectively) species [48–50]. This is concomi-

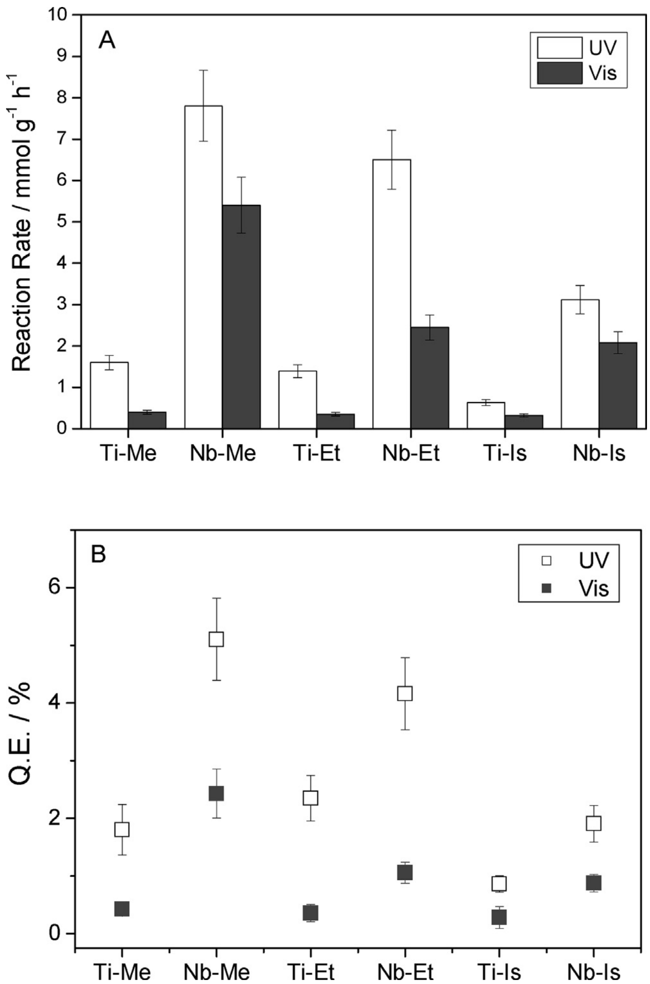

Fig. 4. Reaction rate (A) and quantum efficiency (B) of the hydrogen photo-production using different alcohols. Me, Et and Is stand for methanol, ethanol and 2-propanol (isopropanol).

tantly observed with the decrease of isolated hydroxyl of titania at ca. 3693 cm^{-1} as well as the decreasing of the water (and interacting hydroxyl radicals) signals at ca. 3650-3200 and 1640 cm^{-1}. C—O stretching bands for these two (methanol/methoxy) adsorbate species appear around 1051 cm^{-1} but the bands are so broad that cannot be easily resolved. Additional peaks in the ca. 1500–1100 cm^{-1} region are indicative of the formation of other species. Although the region around 1450 cm^{-1} has contribution from methanol/methoxy species, the presence of peaks at ca. 1370-1350, 1205, and 1165–1145 cm^{-1} indicate the formation of carboxylate or carbonate species [50–53]. In view of the relative similitude observed in these frequencies after the saturation with the ethanol:water mixture, the dominance of carbonate species may be inferred if such results are jointly considered with the selectivity data collected for methanol and ethanol in Table 2. In the case of ethanol (central row in Figs. 5 and 6), the C—H region showed peaks at ca. 2977-2975, 2930, 2900 and 2875 cm^{-1} for both (Ti and Nb) samples. Additional bands related to the alcohol are presented at ca. 1382-1279 (δasCH_3), 1140 (C—C stretch) and 1092-1089 and 1055-1048 (C—O stretch) cm^{-1} [25,54]. The C—O stretch doublet also provides evidence of ethanol and ethoxy species in both Ti and Nb samples. As mentioned, other bands (particularly around 1450 and 1390–1380 cm^{-1}) indicate the presence of carboxylate species but mainly carbonate species formed during the contact of the alcohol and the surface. Additional (negative) contributions are, as occurring with methanol, related to hydroxyls and/or water. Note that the same type of isolated hydroxyl radical (3693, 3700 cm^{-1}) interact with the alcohol in the case of methanol and ethanol. Some differences are, however, observed in the 3600–3000 cm^{-1} region concerning water and/or interacting hydroxyls. Differences between ethanol and methanol in this region would be related to the different alcohol coverage at the surface and the competition with water [46,51–54]. In the case of 2-propanol and for both samples, bands at 2972, 2932-2930, and 2868–2864 cm^{-1} (νCH), 1468 cm^{-1} (δasCH_3), 1380 cm^{-1} (δsCH_3) and δCH mode at 1282 cm^{-1} were observed with several band assigned to the CO stretch vibration mode in the 1175–1130 cm^{-1} region [55,56]. The latter (C—O) bands describe the variety of interactions of the alcohol and the surface, generating several (more than 2) 2-propanol and propoxide species. It is relatively difficult to observe other products at the initial contact of the 2-propanol and the catalysts.

Under reaction conditions (illumination) the consumption of the alcohols (in the three cases here tested) is rather visible (negative bands) in the region of the C—H and C—O stretching vibration modes. All adsorbed species (alcohol and alcoxy species) are consumed and/or desorbed from the surface of the Ti and Nb samples. In the case of methanol, Ti displays appearance (bands with positive intensity) of new bands at 1191, 1388, 1515 and 2868 cm^{-1} while Nb shows new contributions at 1122, 2865, 2963 and a broad band at ca. 1400 cm^{-1}. The ca. 1120–1190 cm^{-1} peaks would indicate the formation of a carbonyl species while the 1515–1400 cm^{-1} would suggest the formation of formate and, less likely, other carboxylate species [48–53]. This indicates that the surface species detected by infrared agrees with detection of formic acid as main product of the methanol transformation. As mentioned, distinctive of the methanol case with respect to other alcohols is the detection of carbonyl species at the surface of both catalysts. Aldehydes may evolve from the (activated) carbonyl species detected (1190–1120 cm) although formaldehyde is only observed at the gas phase in the case of the Nb sample under UV illumination. The detection of (adsorbed) methyl formate is on the other hand not obvious as the most characteristic bands at ca. 1200 and 1750 cm^{-1} [57] were not observed. In the case of ethanol, and for both samples we observe bands at ca. 2950, 1500-1402, 1367-1260 and ca. 1294 cm^{-1} strongly indicative of carboxylate (and carbonate) moieties including formates [48–53]. Finally, in the case of 2-propanol we encountered a relatively similar situation with bands at ca. 2955-2954, 1444 and 1351 cm^{-1}. The absence of bands around/above 1500 cm^{-1} would indicate the lower importance of carboxylates (particularly formate species) [55,56]. Note that we cannot detect acetone (no hint around or above 1650 cm^{-1}), but this is not an uncommon situation due to the strong interaction that 2-propanol has with titania surfaces. Such a strong interaction (with respect to reaction products) drives to a rather small coverage for other chemical compounds and particularly acetone [55,56,58].

Overall, under reaction we see the production of carboxylate/carbonate species as the main surface product in the case of methanol and ethanol, indicating that the hole attack to the alcohol would end up in the formation of oxidized species related to the corresponding alcohol/alcoxy adsorbed species. In the case of methanol, carboxylate species generate formic acid and methyl formate. The latter is produced by interaction of the carboxylate and one methanol molecule [57]. For ethanol the carboxylate or carbonate species only end up in the formation of ethyl acetate (Table 2). For methanol, surface carbonyl species were additionally detected but only in one case (Nb under UV illumination) the formation of the aldehyde was observed as a product (Table 2). In the case of 2-propanol the carboxylate-type species are apparently less present at the surface of both Ti and Nb materials, likely due to the low coverage of products and the relatively easy desorption of the main reaction product, acetone. In any case, we also observed evolu-

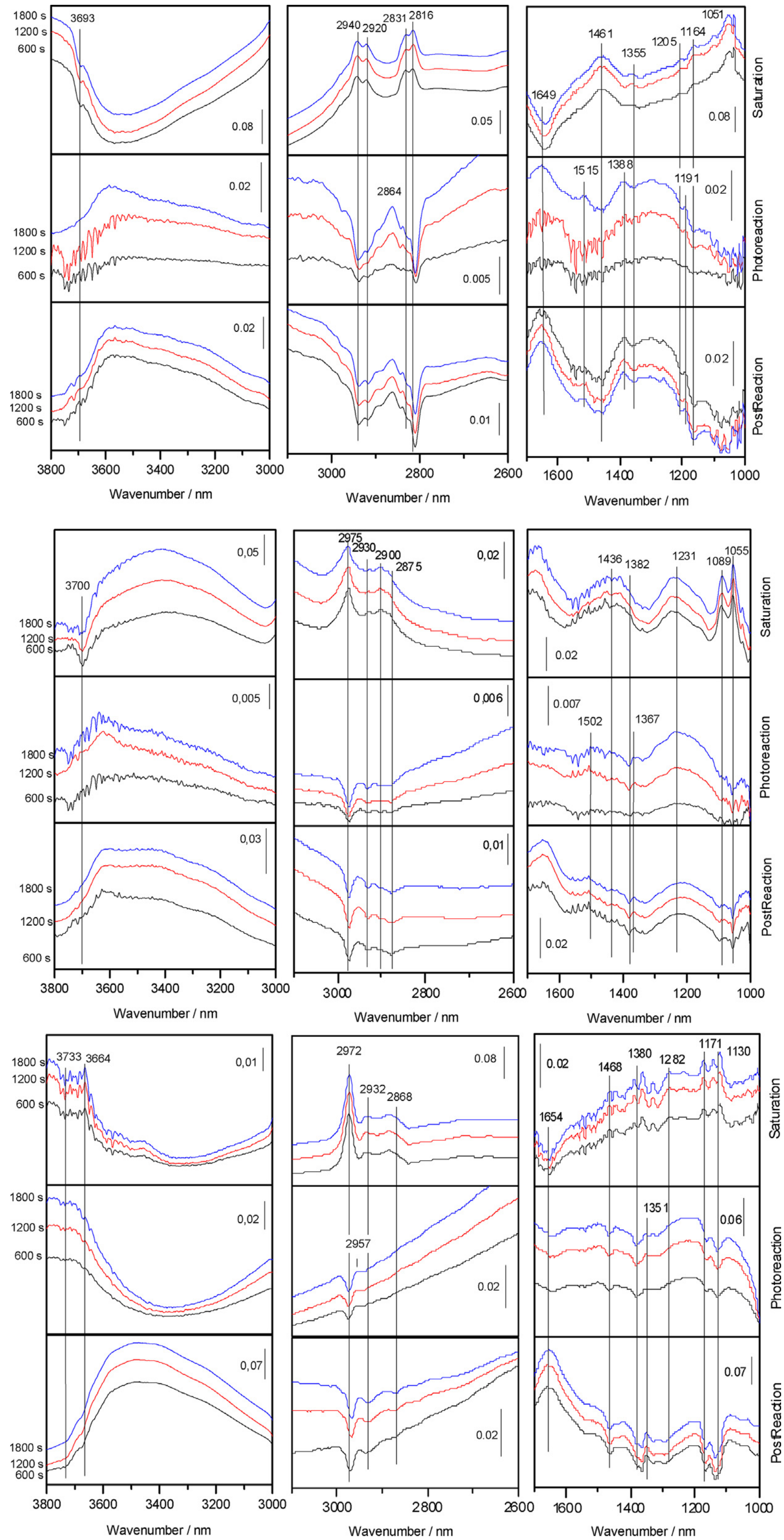

Fig. 5. DRIFTS spectra for the in situ analysis of the methanol (upper panel), ethanol (middle panel) and 2-propanol (lower panel) photo-transformation occurring under reaction conditions for the Ti sample. Spectra obtained during saturation (dark conditions) with the alcohol:water mixture, under reaction-illumination conditions and subsequently at dark (post-reaction) conditions are presented.

tion of the acetone. The propanone-diisopropyl-acetal molecule is formed by reaction of acetone and two molecules of 2-propanol [59].

To further progress in the analysis of the effect of the alcohol chemical nature we discuss the influence of their physico-chemical properties on hydrogen photo-production. The importance of the interaction of lone pairs of the OH groups with unoccupied Ti

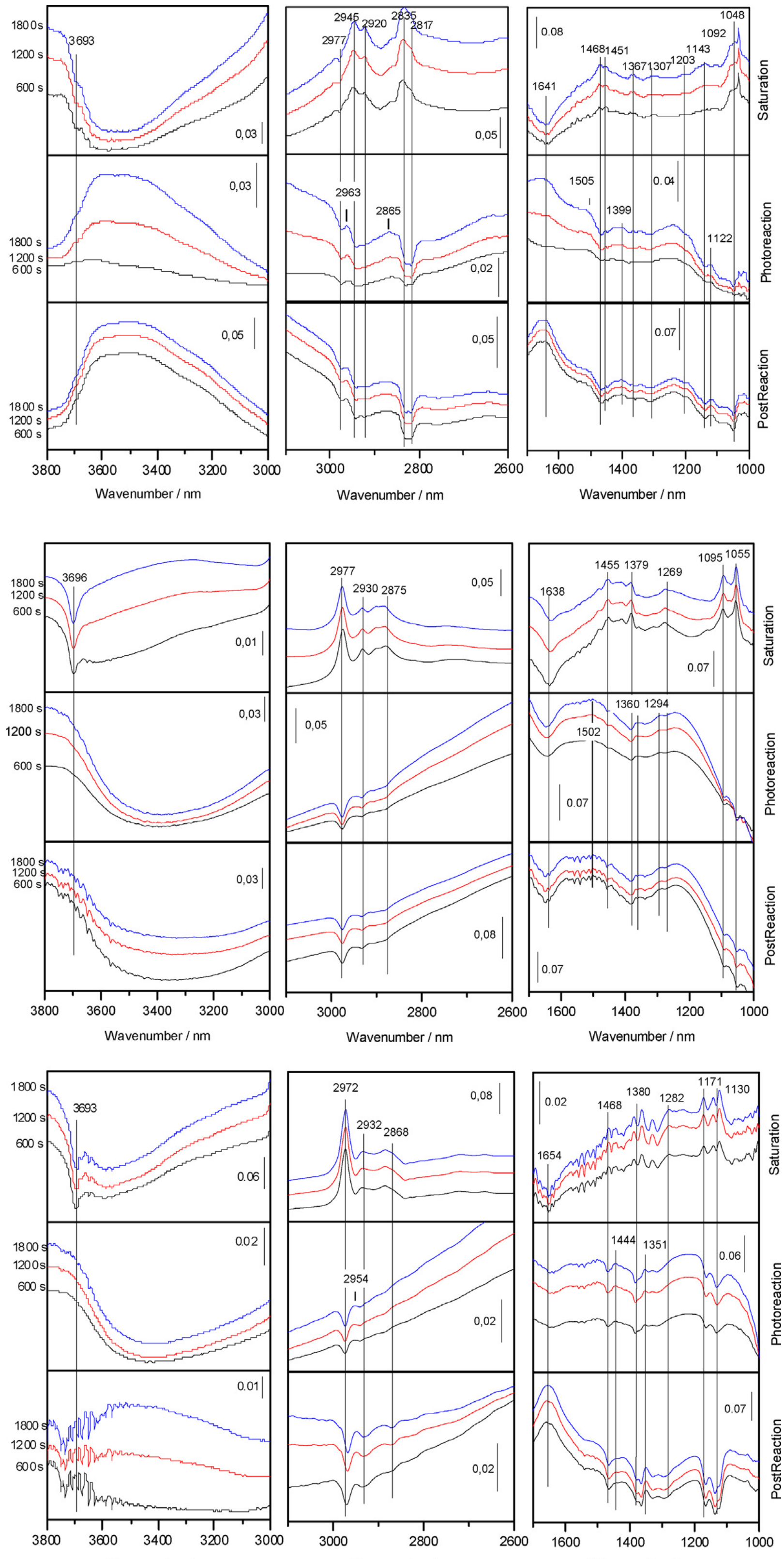

Fig. 6. DRIFTS spectra for the in situ analysis of the methanol (upper panel), ethanol (middle panel) and 2-propanol (lower panel) photo-transformation occurring under reaction conditions for the Nb sample. Spectra obtained during saturation (dark conditions) with the alcohol:water mixture, under reaction-illumination conditions and subsequently at dark (post-reaction) conditions are presented.

3d states to activate the alcohol molecule suggests that alcohol polarity may influence activity, as suggested previously by several authors [40,41,60]. However, methanol markedly differs from the expected tendency if polarity drives photo-activity for hydrogen production. This point has been argued to be based in chemical differences concerning, in first place, the CO production [41].

CO can play a series of roles depending of its quantity as well as its handling at the metal-support interface, which could be positive for hydrogen production through the water gas shift reaction [48], but can be a poison at the surface of the metal with detrimental effects in photo-activity [61]. Whatever the role of the CO in the reaction is, here we do not detect such molecule using infrared while for other catalysts it has been detected in similar experimental conditions [50]. Also, a different alcohol oxidation mechanism was proposed for methanol. This is based in the easy formation and surface stability (or no easy evolution) of formate species created from methanol with respect to other carboxylates or (hydrogen)-carbonates formed from higher alcohols [41]. However, at least when comparing methanol with ethanol using infrared spectroscopy, we show essentially the same behavior of the titania surfaces against the alcohol and evolving molecules coming from the hole-attack. In these two cases, the alcohol evolution seems to proceed initially through a stepwise mechanism with no change in the chain length with consecutive (hole-attack) steps such as: alcohol (alcoxy) → aldehyde (carbonyl-related species) → acid (carboxylates). As mentioned, carboxylate species also evolve forming methyl formate and ethyl acetate. Such a mechanism has been previously proposed [35]. Thus, we can dismiss the formate vs. other carboxyaltes hypothesis as being of primary significance in our case.

Alternatively or in parallel, some authors highlight the significance of thermodynamic issues of the alcohol oxidation step(s) in driving hydrogen photo-production. According to current theories of electron transfer reactions between an electron donor and valence band holes in a semiconductor [41,62], the experimental rate constant (k_{exp}) for such reactions can follow the relation:

$$K_{exp} \propto e^{-\left(E^0_{VB(TiO_2)} - E^0_{ox}\right)/RT} \tag{9}$$

Where $E^0_{VB(TiO_2)}$ is the valence band potential of titania and E^0_{ox} is the oxidation potential of the donor, which according to the discussion presented in the introduction (Eqs. (1)–(4)) is the alcohol. If this charge transfer controls the reaction rate we can expect a linear relationship between the k_{exp} expression in Eq. (9) and the hydrogen photo-production rate (which, by the way, takes place at constant temperature in our experiments). On the other hand, note that, in this study and using our samples, we showed that the rate is also a real measurement of the reaction (quantum) efficiency. Of course, a real calculation should take into account the different products formed during the reaction and the corresponding thermodynamic values. This is a consequence of the fact that hydrogen is extracted from the alcohol molecule in each step of the equations considered in Table 3, as mentioned in the introduction [36,38]. Concretely, E^0_{ox} is calculated (equal to $(-)\Delta G°/nF$, being the Faraday constant F = 96.485 kC mol^{-1}.) from the standard Gibbs energy of alcohol oxidation ($\Delta G°$) and the number of charge species (n) involved in the reaction. These parameters are presented in Table 3 and were calculated using tabulated values of the Gibbs energies and the balance equations also presented in such table [63]. As mentioned, for each alcohol we consider the selectivity to the different (alcohol) oxidation products and thus for each sacrificial molecule we obtained an average value for its E^0_{ox} parameter (Table 4). It is important to note that, this average allows to obtain different values for different illumination sources, a fact required by our (and in general for all) catalytic experiments. The E^0_{ox} parameter values are plotted against the hydrogen production rate in Fig. 7 for the different alcohols and illumination conditions here tested.

In Fig. 7 we observed a quasi-linear trend for the two samples and illumination conditions. This suggests that, for all cases, the rate is dominated by thermodynamic reasons and that the active center and mechanism do not suffer strong differences or variations in terms of the alcohol nature within our series. It should be pointed out that the three alcohols have hydrogen in alpha position of the hydroxyl moiety but show marked differences in the hydrogen photo-production rate. In particular, we note that methanol fits in the linear trends, similarly to the other alcohols. This strongly suggests the similar role and evolution of the alcohol in the photo-production of hydrogen, irrespective of the sample and excitation wavelength.

Table 4
Average oxidation potential (equation **Eox = -ΔG°/(n·F)**) for the different alcohol reactions taking place in the reactor for the different catalysts and illumination conditions.

Catalyst	Illumination	Alcohol	E°ox. (V) versus NHE[a]
Nb	UV	Methanol	0.037
	Vis		0.044
Ti	UV		0.042
	Vis		0.052
Nb	UV	Ethanol	0.112
	Vis		0.119
Ti	UV		0.101
	Vis		0.092
Nb	UV	2-propanol	0.241
	Vis		0.213
Ti	UV		0.143
	Vis		0.143

[a] Average standard error; 8.7%.

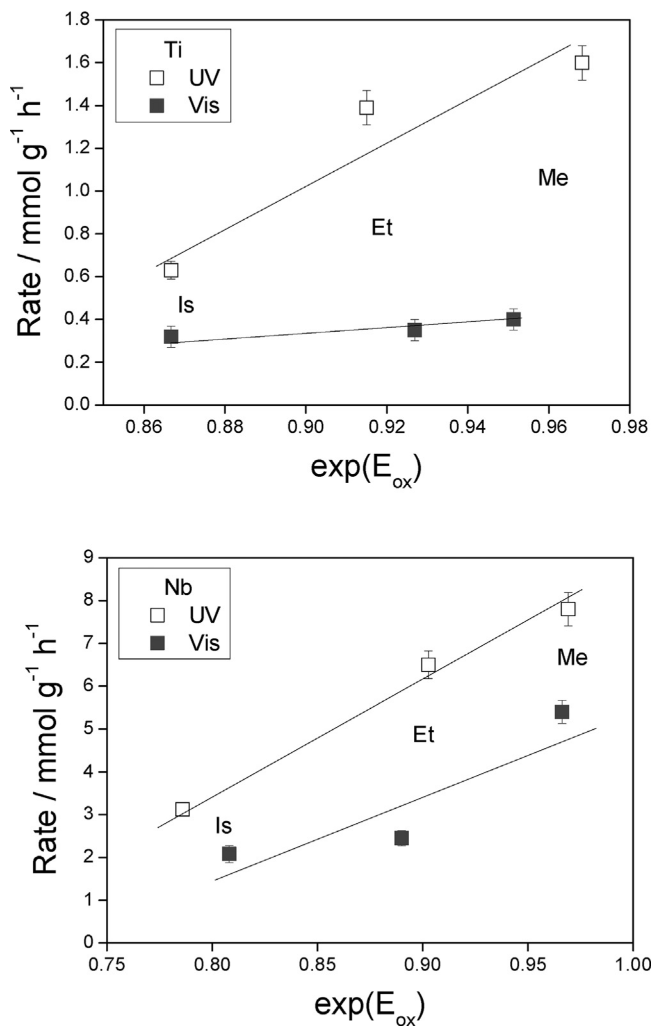

Fig. 7. Rates of H_2 production versus exp(Eox.) of the alcohol.

4. Conclusions

In this contribution we examine the photo-production of hydrogen from bio-alcohol molecules using bare anatase and Niobium-doped anatase materials having a 0.5 wt% Pt as co-catalyst. These materials have similar morphological properties (particularly BET surface area and primary particle size of the noble metal and anatase components). Three alcohol molecules, methanol, ethanol, and 2-propanol, and two illumination sources corresponding to UV and visible ranges were utilized. Catalytic output was measured through the reaction rate and the true quantum efficiency observables. The parallel behavior of both observables along our sample series indicates that the reaction rate renders a realistic measurement of the catalytic properties of the solids. The Niobium-doped sample presented an improved performance under all experimental conditions tested, proving quantum efficiency values going from ca. 1–5%. Enhancement ratios from 1.8 to 2.8 were observed with respect to the titania reference system.

For all illumination conditions and samples we interpret catalytic activity in hydrogen production with the combined use of an in-situ infrared study as well as the thermodynamic foundation of the reaction rate. From a mechanistic point of view we observed differences between alcohols but those are of minor relevance to justify quantitatively the differences appearing in hydrogen production rates using the three alcohols here studied. Differences in activity were correlated quantitatively with the average oxidation potential of the alcohol if the selectivity in the bio-molecule oxidation is taken into account to interpret hydrogen photo-production. For all samples and illumination conditions here tested, the work showed that the thermodynamic of the interaction between the solid(s) and the sacrificial molecule is likely driving the catalytic output and interprets the different rates and quantum efficiency values obtained.

Acknowledgements

We are thankful to MINECO (Spain) for supporting the work carried out through the ENE2016-77798-C4-1-R grant. We thanks Dr. Rodriguez-Ramos group for performing HPLC analysis of liquid samples.

References

[1] N. Vecirolu, F. Barbir, Int. J. Hydrogen Energy 17 (1992) 391–404.
[2] X. Chen, S.S. Chen, L. Guo, S.S. Mao, Chem. Rev. 110 (2010) 6503–6570.
[3] K. Maeda, K. Domen, J. Phys. Chem. Lett. 1 (2010) 2655–2661.
[4] A. Kubacka, M. Fernández-García, G. Colón, Chem. Rev. 112 (2012) 1555–1614.
[5] K. Villa, X. Domenech, S. Malato, M.I. Maldonado, J. Peral, Int. J. Hydrogen Energy 38 (2013) 12718–12724.
[6] Y. Ma, X. Wang, Y. Jia, X. Chen, H. Han, C. Li, Chem. Rev. 114 (2014) 9987–10043.
[7] J.C. Colmenares, R. Luque, Chem. Soc. Rev. 43 (2014) 765–778.
[8] X. Li, J. Yu, J. Low, Y. Fang, J. Xiao, X. Chen, J. Mater. Chem. A 3 (2015) 2485–2534.
[9] J.C. Colmenares, Nanophotocatalysis in selective transformations of lignocellulose-derived molecules: a green approach for the synthesis of fuels, fine chemicals, and pharmaceuticals, in: Nurxat Nuraje, Ramazan Asmatulu, Guido Mul (Eds.), Green Photo-active Nanomaterials: Sustainable Energy and Environmental Remediation, The Royal Society of Chemistry, Warsaw, 2016, pp. 168–201 (chap. 8).
[10] Y. Li, G. Ma, S. Peng, G. Lu, S. Li, Appl. Surf. Sci. 254 (2008) 6831–6836.
[11] M.A. Khan, S.I. woo, O.B. Yang, Int. Hydrogen Energy 33 (2008) 5345–5351.
[12] X. Sun, H. Liu, J. Dong, J. Wei, Y. Zhang, Catal. Lett. 135 (2010) 219–225.
[13] S. Piskuniv, O. Lisovski, J. Begens, M. Wessel, E. Spohr, J. Phys. Chem. C 119 (2015) 18686–18696.
[14] O. Fontelles-Carceller, M.J. Muñoz-Batista, J.C. Conesa, M. Fernández-García, A. Kubacka, Appl. Catal. B 216 (2017) 133–145.
[15] U. Caudillo-Flores, M.J. Muñoz-Batista, J. Cortés, M. Fernández-García, A. Kubacka, Mol. Catal. 437 (2017) 1–10.
[16] J.C. Colmenares, A. Magdziarz, M.A. Aramendia, A. Marinas, J.M. Marinas, F.J. Urbano, J.A. Navío, Catal. Commun. 16 (2011) 1–6.
[17] T. Kawan, T. Sakata, Nature 286 (1980) 474–476.
[18] A. Galinska, J. Walendziewski, Energy Fuels 11 (2005) 1143–1147.
[19] Y.X. Li, Y.Z. Me, S.Q. Peng, G.X. Lu, S.B. Li, Chemosphere 63 (2006) 1312–1318.
[20] A. Pastora, D.I. Kondarides, X.E. Verykios, Catal. Today 124 (2007) 94–102.
[21] X. Fu, J. Long, X. Wang, D.C.Y. Leung, Z. Ding, L. Wu, Z. Zhang, Z. Li, X. Fu, Int. J. Hydrogen Energy 33 (2008) 6484–6491.
[22] W. Sun, S. Zhang, Z. Liu, W. Wang, Z. Mao, Int. J. Hydrogen Energy 33 (2008) 1112–1117.
[23] M. Bouker, Catal. Lett. 142 (2012) 923–929.
[24] Y. Ma, Q. Xu, X. Zong, D. Wang, G. Wu, X. Wang, C. Li, Energy Environ. Sci. 5 (2012) 6345–6351.
[25] E. Pulido Melián, J.A. Ortega Méndez, C. Rodríguez López, M. Nereida Suárez, J.M. Doña Rodríguez, J.A. Navío, D. Fernández Hevia, Int. J. Hydrogen Energy 38 (2013) 11737–11748.
[26] D. Slament, V. Tristanidi, M. Ibadurrbhran, Energy Res. 37 (2013) 1372–1381.
[27] G.N. Nomikos, P. Panagiotopoulous, D.I. Kondarides, X.E. Verykios, Appl. Catal. B 146 (2014) 249–257.
[28] A. Kubacka, M.J. Muñoz-Batista, M. Fernández-García, S. Obregón, G. Colón, Appl. Catal. B 163 (2015) 214–222.
[29] S. Obregón, M.J. Muñoz-Batista, M. Fernández-García, A. Kubacka, G. Colón, Appl. Catal. B 179 (2015) 468–478.
[30] Y.-J. Yuan, J.-R. Tu, Z.-J. Ye, Z.-T. Yu, Z.-G. Zou, Appl. Catal. B 188 (2016) 13–22.
[31] Z. Chen, X. Jian, C. Zhu, C. Shi, Appl. Catal. B 199 (2016) 241–251.
[32] Q. Hu, J. Huan, G. Li, J. Chen, Z. Zhang, Z. Deng, Y. Jiang, W. Guo, Y. Cao, Appl. Surf. Sci. 369 (2016) 201–206.
[33] M. Zhang, R. Sun, Y. Li, Q. Shi, L. Xie, J. Chen, X. Xu, H. Shi, W. Zhao, J. Phys. Chem. C 120 (2016) 10746–10756.
[34] J.G. Highfield, M.H. Chen, P.T. Ngyen, Z. Chen, Energy Environ. Sci. 2 (2009) 991–1002.
[35] G.L. Chiarello, M.H. Aguirre, E. Selli, J. Catal. 273 (2010) 182–190.
[36] T.A. Kandiel, I. Ivanova, D.W. Bahnemann, Energy Environ. Sci. 7 (2014) 1420–1426.
[37] A. Naldom, M.D. Ángelo, M. Altomare, M. Morelli, R. Scott, F. Morazzoni, E. Selli, V. Del Santo, Appl. Catal. B 130–131 (2013) 239–248.
[38] Galinska, J. Walendziewski, Energy Fuels 19 (2005) 1143–1147.
[39] C.R. López, E. Pulido Melián, J.A. Ortega Méndez, J.M. Doña Rodríguez, O. González Díaz, J. Photochem. Photobiol. A 312 (2015) 45–54.
[40] W.-T.- Chen, A. Chan, Z.H.N. Al-Azri, A.G. Dosado, M.A. Nadeem, D. Sun-Waterhouse, H. Idriss, G.I.N. Waterhouse, J. Catal. 329 (2015) 499–513.
[41] Z.H.N. Al-Azri, W.-T.- Chen, A. Chan, V. Jovic, T. Ina, H. Idriss, G.I.N. Waterhouse, J. Catal. 329 (2015) 355–367.
[42] G.K. Willianson, W.H. May, Acta Metall. 1 (1953) 22–29.
[43] P. Kubelka, J. Opt. Soc. Am. 38 (1948) 448–457.
[44] M. Fernández-García, A. Martínez-Arias, J.C. Hanson, J.A. Rodriguez, Chem. Rev. 104 (2004) 4063–4105.
[45] S.E. Braslavsky, A.M. Braun, A.E. Cassano, A.V. Emeline, M.I. Litter, L. Palmisano, V.N. Parmon, N. Serpone, Pure Appl. Chem. 83 (2011) 931–1014.
[46] M.J. Muñoz-Batista, A. Kubacka, A.B. Hungría, M. Fernández-García, J. Catal. 330 (2015) 154–166.
[47] M.L. Satuf, R.J. Brandi, A.E. Cassano, O.M. Alfano, Ind. Eng. Chem. Res. 44 (2005) 6643–6649.
[48] A. Yamakata, T.-A. Ishibashi, H. Onishi, J. Phys. Chem. B 106 (2002) 9122–9125.
[49] P.A. Panatoyov, S.T. Burrows, J.P. Morris, J. Phys. Chem. C 116 (2012) 6623–6635.
[50] O. Fontelles-Carceller, M.J. Muñoz-Batista, E. Rodríguez-Castellón, J.C. Conesa, M. Fernández-García, A. Kubacka, J. Catal. 347 (2017) 157–169.
[51] A. Matson, L. Osterlund, J. Phys. Chem. C 114 (2010) 14121–14132.
[52] A.C. Sola, D. Garzón Sousa, J. Araña, O. González Díaz, J.M. Doña Rodríguez, P. Ramírez de la Piscina, N. Homs, Catal. Today 266 (2016) 53–61.
[53] C.E. Naroyakkara, J.K. Dillon, V.H. Grassian, J. Phys. Chem. C 118 (2014) 25487–25495.
[54] D.L. Carvalho, L.E.P. Borges, L.G. Appel, P. Ramírez de la Piscina, N. Homs, Catal. Today 213 (2013) 115–121.
[55] F. Arsac, D. Bianchi, J.M. Chovelon, A.C. Ferronato, J.M. Herrmann, J. Phys. Chem. A 110 (2006) 4202–4212.
[56] F. Arsac, D. Bianchi, J.M. Chovelon, C. Ferronato, J.M. Herrmann, J. Phys. Chem. A 110 (2006) 4213–4222.
[57] M. El-Roz, Ph. Bazin, Phys. Chem. Chem. Phys 17 (2015) 11277–11285.
[58] M.J. Muñoz-Batista, U. Caudillo-Flores, F. Ung-Medina, M.C. Chávez-Parga, J.A. Cortés, A. Kubacka, M. Fernández-García, Appl. Catal. B 201 (2016) 400–410.
[59] H. Maarse, Volatile Compounds in Foods and Beverages, 1991, New York.
[60] Y.Z. Yang, C.H. Chang, H. Idriss, Appl. Catal. B Environ. 67 (2006) 217–222.
[61] G.H. Haselman, D. Elder, ACS Catal. 7 (2017), 4688–4675.
[62] V. Balzani, F. Scandola, in: Michael Gratzel (Ed.), Energy Resources Through Photochemistry and Catalysis, Academic Press Inc, New York, 1983, pp. 2–48.
[63] J.A. Dean, (Ed.) Langeís Handbook of Chemistry, 15th ed. 1999, New York.